IOP Conf. Series: Journal of Physics: Conf. Series **854** (2017) 012032 doi:10.1088/1742-6596/854/1/012032

Comparative study on the wake deflection behind yawed wind turbine models

Jannik Schottler[1], Franz Mühle[2], Jan Bartl[3], Joachim Peinke[1], Muyiwa S Adaramola[2], Lars Sætran[3], Michael Hölling[1]

[1] ForWind, University of Oldenburg, Institute of Physics, Oldenburg, Germany
[2] Faculty of Environmental Sciences and Natural Resource Management, Norwegian University of Life Sciences, Ås, Norway
[3] Department of Energy and Process Engineering, Norwegian University of Science and Technology, Trondheim, Norway

E-mail: jannik.schottler@forwind.de

Abstract. In this wind tunnel campaign, detailed wake measurements behind two different model wind turbines in yawed conditions were performed. The wake deflections were quantified by estimating the rotor-averaged available power within the wake. By using two different model wind turbines, the influence of the rotor design and turbine geometry on the wake deflection caused by a yaw misalignment of 30° could be judged. It was found that the wake deflections three rotor diameters downstream were equal while at six rotor diameters downstream insignificant differences were observed. The results compare well with previous experimental and numerical studies.

1. Introduction

In order to reduce power losses in wind farms caused by wake effects, different active wake control strategies were investigated in the recent years. One promising approach is an intentional yaw misalignment which is able to deflect the wake deficit laterally and thus reduce its impact on downstream turbines. However, a detailed understanding of a yawed wind turbine's wake trajectory is needed before potentially applying the concept.

As full-scale field studies are limited and numeric simulations face modeling uncertainties, wind tunnel experiments are a useful tool for validation purposes. Wakes of yawed model wind turbines have been addressed in multiple wind tunnel studies using different model turbines of varying geometries and rotor designs. For a small model of $D = 0.12\,m$ and a yaw angle of $\gamma = 30\,°$, Medici and Alfredsson [1] found a wake deflection of about $z/D \approx 0.5$ at a downstream distance of $x/D = 4$. For the same yaw angle, Krogstad and Adaramola [2] measured a wake deflection of $z/D \approx 0.2$ rotor diameters already at $x/D = 1$. The model turbine, however, had a rotor diameter of D=0.90 m and thus was significantly larger. A slightly different wake deflection angle for $\gamma = 30°$ was found in an experimental PIV study by Bastankhah and Porté-Agel [3], who localized the wake center at $z/D \approx 0.16$ for x/D=2 and at $z/D \approx 0.34$ for x/D=6 downstream distance for a smaller wind turbine model of D=0.15 m. Howland et al. [4] used a yawed drag disc of D=0.03 m and found a deflection between $z/D \approx 0.4$ and $z/D \approx 0.5$ at a distance of $x/D = 6$, dependent on the measurement technique and fitting method. All of these studies qualitatively showed consistent wake deflection effects, that can be generalized. However,

certain quantitative differences in the deflection can be observed. Several factors could influence the variation in the quantification of the wake deflection. First of all, the airfoil dependent force coefficients are different for the rotors, giving a different initial forcing on the air deflected around the turbines' blades. Secondly, the tower and nacelle geometries of the different model turbines are deemed to have a certain influence to interact with the flow. A third factor could be inflow and boundary conditions in different wind tunnel environments. Furthermore, Howland et al. [4] show a significant influence of the 2- or 3-dimensional fitting method on the wake deflection.
In order to judge effects of boundary conditions such as turbine geometry, blade design or wind tunnel blockage, comparative wake measurements behind two different model turbines developed at ForWind in Oldenburg and at the NTNU in Trondheim were performed. The models vary in size, geometry and blade design. Other dimensionless parameters of the setup such as tip speed ration (TSR) are equal, allowing for an isolation of effects caused by the turbine type. This paper describes the experimental setup and methods used in detail. Further, the wake deflection during a yaw misalignment of $\gamma = -30^\circ$ is quantified for both turbines at two downstream distances using an approach estimating the available power of a potential downstream turbine.

2. Experimental setup

2.1. Wind tunnel facility & inflow conditions

The experiments were conducted at the closed-loop wind tunnel at the Norwegian University of Science and Technology (NTNU) in Trondheim, Norway. The test section is 11.15 m long with an inlet cross-section of 2.71 m × 1.81 m (width × height). During the experiments a shear-flow-generating turbulence grid was installed at the inlet to the test section, which is described by Bartl & Sætran in detail [5]. The installed turbulence grid generates a vertical shear in the inflow velocity, being non-uniform over the rotor area. A common way to describe wind shear is the power law [6]

$$\frac{u}{u_{ref}} = \left(\frac{y}{y_{ref}}\right)^{\alpha}, \tag{1}$$

which expresses the wind speed u as a function of height y, given that the wind speed at an arbitrary reference height y_{ref} is known. The coefficient α describes the strength of shear in the profile. The shear grid used here generates a profile that can be approximated by a shear coefficient of $\alpha = 0.11$, which is a realistic value for offshore boundary layers in stable atmospheric conditions [7]. Table 1 gives an overview of the inflow conditions for each turbine. The turbulence intensity,

$$TI = \frac{\sigma_u}{\langle u \rangle}, \tag{2}$$

and the free stream velocity u_∞ refer to the respective turbine's hub height.

Table 1. Overview of the inflow conditions at each turbine's location for the empty wind tunnel. α corresponds to Eq. (1), u_∞ and TI refer to the data at the respective hub height.

Turbine	u_∞ [ms^{-1}]	TI [%]	α [–]	Hub height [m]
ForWind	7.5	5.2	0.11	0.820
NTNU	10	10.1	0.11	0.890

2.2. Model wind turbines

Two different model wind turbines were used that vary in size, blade design and geometry. The turbines will be denoted *NTNU* and *ForWind*, respectively. The ForWind turbine has a rotor diameter of $D_{ForWind} = 0.580\,m$ and a hub diameter of 0.077 m. In order to adjust the hub height of the turbine to the center of the NTNU wind tunnel, the turbine tower was extended with four rods of a diameter of 0.02 m attached to the base plate. The rotor blades are based on an SD-7003 airfoil profile, and were manufactured by a vacuum casting method using a MG804 synthetic (isocyanate-polyol) compound. Further details about the blade design and airfoil characteristics can be found in Section 2.3. The rotor is designed for turning in clockwise direction when observed from upstream. The ForWind turbine features an automatic load control, which allows an operation at constant TSR during the experiments. The pitch angle β can be adjusted using a stepper motor (see [8] for details) and was set to have maximum performance in perfect yaw alignment, which resulted in a value of $\beta = 1.8°$ for this experiment. The pitch angle and tip speed ratio were then kept constant when the turbine was yawed to an angle of $\gamma = -30°$. Further details about the load control and the turbine design are described by Schottler et al. [8].

The NTNU turbine has a larger rotor of $D_{NTNU} = 0.894\,m$ with a hub diameter of 0.090 m. It is a re-design of the turbines used in [5], having a thinner tower and a smaller nacelle in order to minimize their effects on the wake flow behind the turbine. The aluminum blades are based on a NREL S826 airfoil, which was designed by the National Renewable Energy Laboratory (NREL). The NTNU rotor turns in counter-clockwise direction and is driven at by a 400W Panasonic LIQI electric servo motor. The servo motor ensures a rotation at constant tip speed ratio, while the excessive power is burned off in an external resistor. The pitch angle of the turbine has to be adjusted manually and was fixed to $\beta = 0°$ for this experiment.

Both model turbines were operated at the same TSR of $\lambda = 6$. Table 2 gives an overview of the main characteristics of both turbines used, Figure 1 shows scaled sketches of both turbine models.

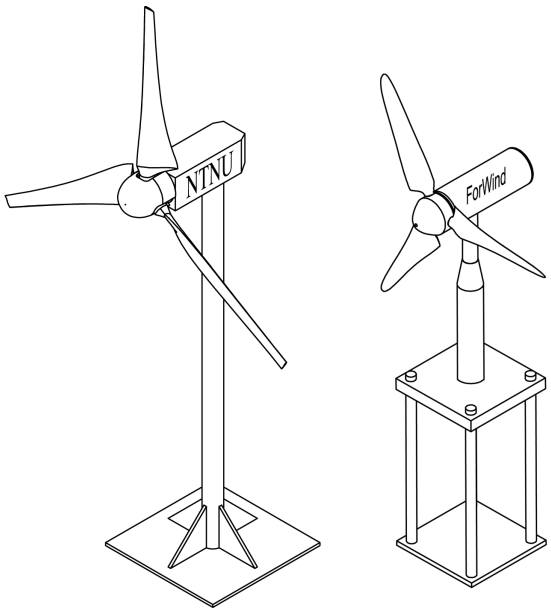

Figure 1. Scaled technical drawings of both model wind turbines. Left: NTNU turbine, right: ForWind turbine.

Table 2. Summary of main turbine characteristics. The TSR is based on the free stream velocity u_∞ at hub height. The Reynolds number at the blade tip, Re_{tip}, is based on the chord length at the blade tip and the effective velocity during turbine operation. The blockage corresponds to the ratio of the rotor's swept area to the wind tunnel's cross sectional area. The direction of rotation refers to observing the rotor from upstream.

Turbine	Rotor diameter	Hub diameter	Blockage	TSR	Re_{tip}	Rotation
ForWind	0.580 m	0.077 m	5.4 %	6	$\approx 6.4 \times 10^4$	clockwise
NTNU	0.894 m	0.090 m	13 %	6	$\approx 1.1 \times 10^5$	counter-clockwise

2.3. Rotor and airfoil comparison

The ForWind rotor has a total twist of about 22° and a chord length distribution varying from about 70 mm at the root to about 20 mm at the tip. The rotor is an upscaled version of the rotor described in Odemark and Fransson [9]. It is build from elements based on the SD-7003 airfoil, which is specifically designed for low Reynolds number operation. A detailed documentation is given by Selig et al. [10] and Counsil et al. [11].

The total twist distribution on the bigger NTNU rotor spans about 38° from the blade root to the tip, while the chord length varies from 82 mm to 26 mm. The rotor geometry is defined in detail by Sætran & Bartl [12] and is based on the NREL S826 airfoil from the root to the tip. The airfoil was originally designed for full-scale wind turbines operating at Reynolds numbers in the order of 10^6 and is documented by Somers [13]. As the Reynolds number for this model experiment is about one order of magnitude lower, experimental performance data were recorded for low to moderate Reynolds numbers. One comprehensive dataset is provided by Sarmast and Mikkelsen [14], another by Ostovan et al. [15].

The airfoil shapes, on which the two rotors are based, as well as the performance at a Reynolds number of $Re = 1 \times 10^5$ are compared in Figure 2. The drag distribution is observed to be very similar for the two airfoils, while the lift force is seen to be around 20% higher for the NREL S826 airfoil for a wide range of angles of attack. This noteworthy difference in lift is the reason for a lower power output of the ForWind rotor, but also implicates a difference in thrust force between the rotors, having an impact of the wake deflections.

2.4. Measurement techniques

Flow velocities in the wake were measured using a DANTEC FiberFlow two-component Laser Doppler Anemometer (LDA) system, recording the u- and v-component of the flow, cf. Figure 4. 5×10^4 samples were recorded at each point of measurement, resulting in time series of varying lengths of approximately 30 s. For one wake measurement, the LDA was traversed in the YZ-plane, cf. Figure 4. Each measured plane consists of 357 points, 21 in z-direction ranging from -D to +D and 17 in y-direction, ranging from -0.8 D to 0.8 D. The resulting distance separating two points of measurement is thus 0.1 D. Figure 3 illustrates the measurement grid behind the rotors.

Based on this grid of physically measured values, a much finer grid of a total of $401 \times 321 \approx 129000$ grid point is interpolated. The distance between the interpolated grid points is thus reduced to 0.005 D. Natural neighbor interpolation is used, which is resulting in a smoother approximation of the distribution of data points [16]. The interpolated values make it possible to calculate a rotor-averaged velocity of approximately 3.16×10^4 data points per rotor area for the wake center detection method described in Section 3.1.

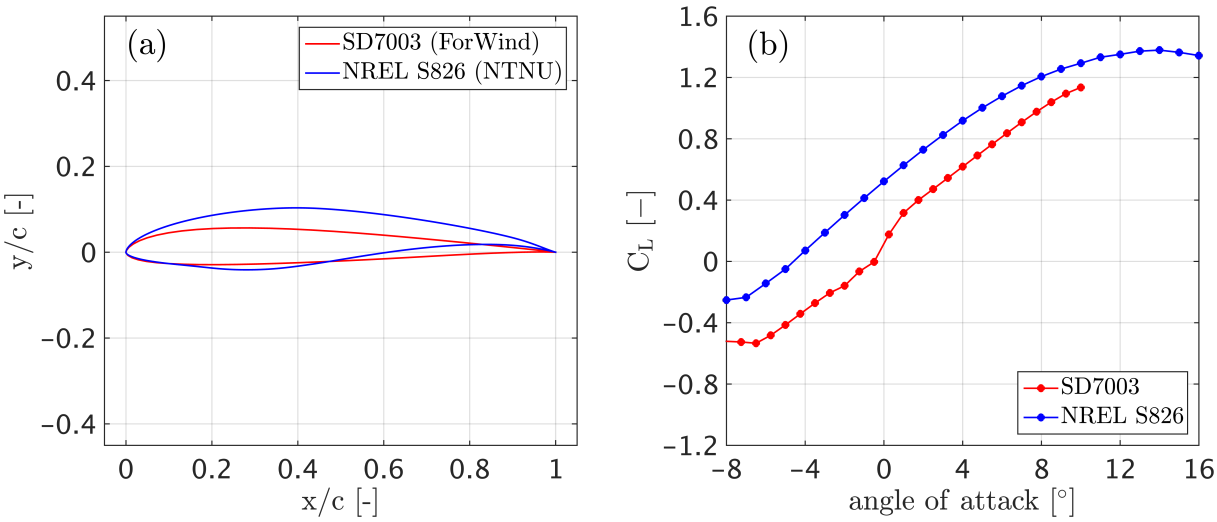

Figure 2. Comparison of the airfoils used at the ForWind and NTNU rotor. **(a)** airfoil shape, **(b)** lift and drag coefficients calculated for $Re = 1 \times 10^5$ using XFoil.

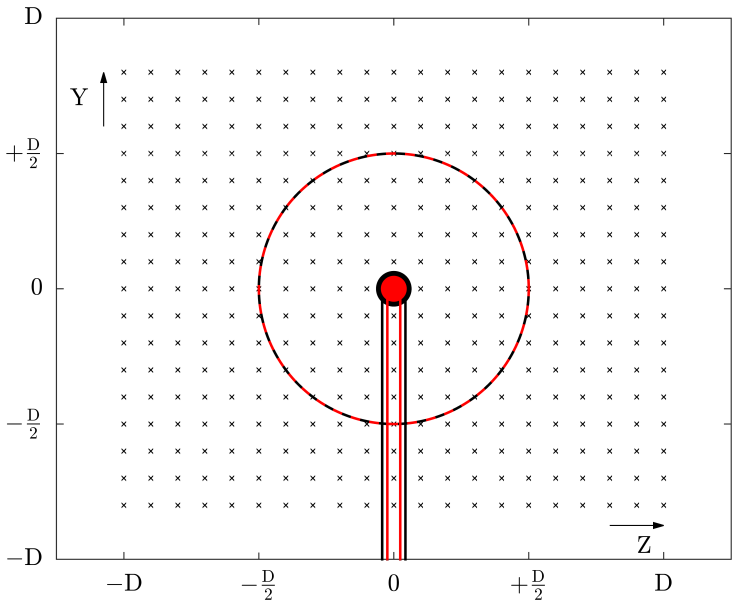

Figure 3. Illustration of the measurement grid behind the model turbines. The tower and hub of the NTNU turbine are marked in red, black corresponds to the ForWind turbine. Measurement positions are marked by ×.

2.5. Setup

The respective model turbines were positioned on a turning table allowing for a yaw misalignment. The orientation of the yaw angle γ is based on the tunnel geometry, which is sketched in Figure 4 along with the schematic setup.

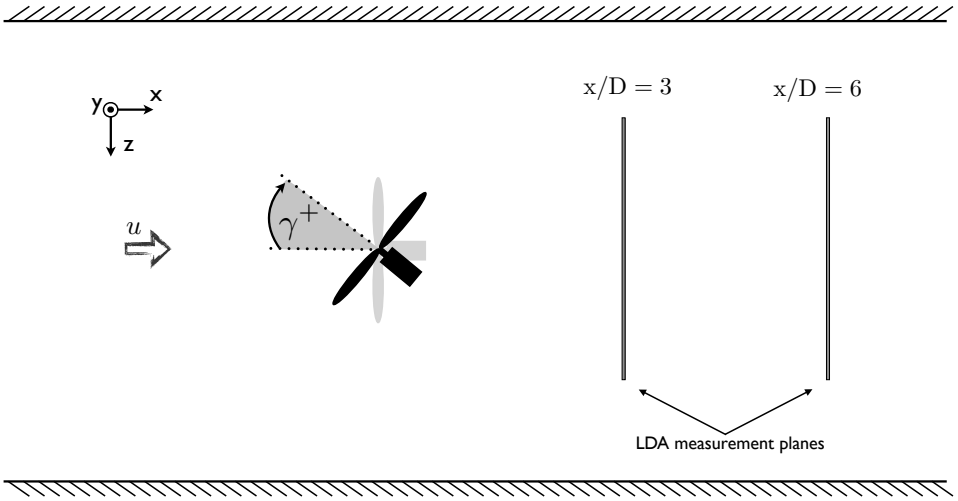

Figure 4. Sketch of the wind tunnel setup, top view. Scales do not match.

3. Methods

3.1. Wake location detection

As a major motivation for studying wind turbine wakes is the effect on downstream turbines, we use the power of a potential downstream turbine for estimating the wake center position in z-direction. A similar approach was shown by Vollmer et al. [17]. The potential power of a downstream turbine is

$$P^* = \sum_{i=1}^{10} \rho A_i \left\langle u_i(t) \right\rangle_{A_i,t}^3 . \tag{3}$$

The rotor area is divided in ten ring segments. A_i is the area of the i^{th} ring segment and $\langle u_i(t) \rangle_{A_i,t}$ denotes the temporally and spatially averaged velocity in main flow direction within the area A_i. For simplicity, the power coefficient is assumed to be constant for each ring segment and is not included here. P^* is estimated for 50 different hub locations in the range $-0.5\,\mathrm{D} \leq \mathrm{z} \leq 0.5\,\mathrm{D}$, at the original hub height. We define the wake center in z-direction by the z position resulting in the minimum of P^*. The procedure is illustrated in Figure 5.

3.2. Operating conditions

Both turbines were operated close to their optimal operation conditions at a yaw angle of $\gamma = 0\,^\circ$. For $\gamma = -30\,^\circ$, the TSR was kept constant at $\lambda = 6$ based on the u-component of the free stream velocity, resulting in a power decrease of approximately 21 % for the ForWind, and 29 % for the NTNU turbine. The average of both values is 25 %, which corresponds precisely to a cosine-squared relation between the relative power and angle of yaw misalignment as $\cos^2(30^\circ) = 0.75$.

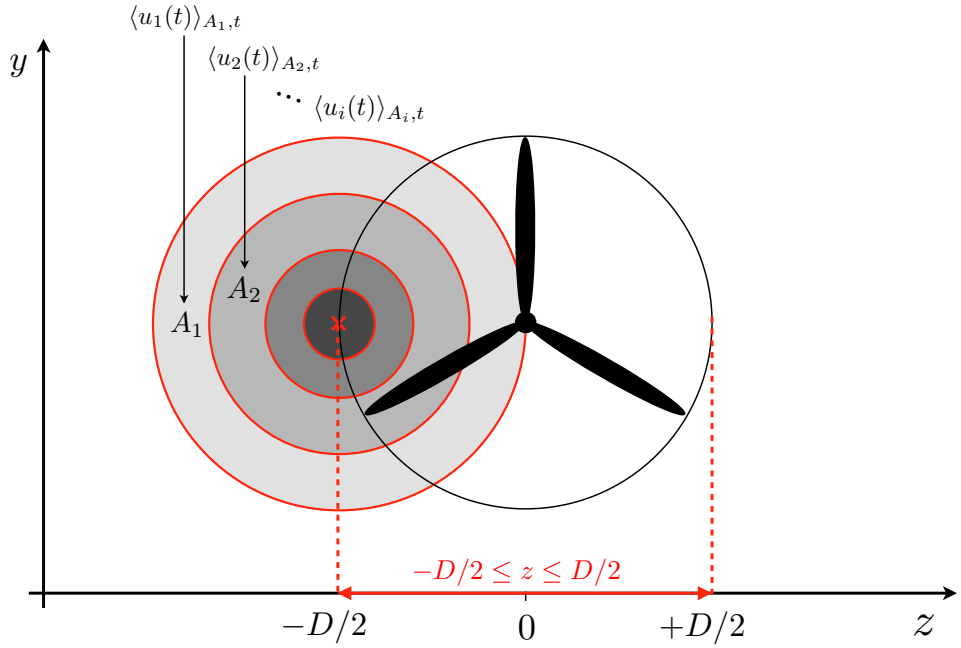

Figure 5. Illustration of the wake center detection method. A_i is the area of the i^{th} ring segment of the potential downstream turbine's rotor area, whose hub is located at the red $\times$. $\langle u_i(t)\rangle_{A_i,t}$ is the spatially and temporarily averaged u-component of the velocity. The potential power P^* is calculated for each ring segment and then added up. This procedure is repeated for various hub locations $\times$, while the position resulting in the lowest value of P^* is interpreted as wake center.

4. Results

For the wakes of both turbines during a yaw misalignment of $\gamma = -30°$, the deflections in z-direction at x/D = 3 and x/D = 6 were quantified using the approach described in Section 3.1. Figure 6 shows the normalized potential power P^* for varying z-positions and both downwind distances. As expected, for both turbines the wake is deflected in z-direction, whereas the magnitude of deflection increases with the downstream distance behind the respective rotor. Table 3 summarizes the results derived from Figure 6 and will be used for further quantification of the wakes' deflections. At x/D=3, the wake deflection magnitude is 0.19 D for both turbines,

Table 3. Wake center location and corresponding skew angles based on Figure 6. The wake location corresponds to the value of z resulting in the lowest value of P^*, cf. Section 4.

Turbine	x/D	Wake location	Skew angle
NTNU	3	0.19 D	$\approx 3.7°$
ForWind	3	0.19 D	$\approx 3.7°$
NTNU	6	0.32 D	$\approx 3.0°$
ForWind	6	0.40 D	$\approx 3.8°$

which results in a wake skew angle of approximately 3.7°. The ForWind turbine shows a steeper graph, corresponding to a more pronounced deficit in the wake center, possibly due to the larger

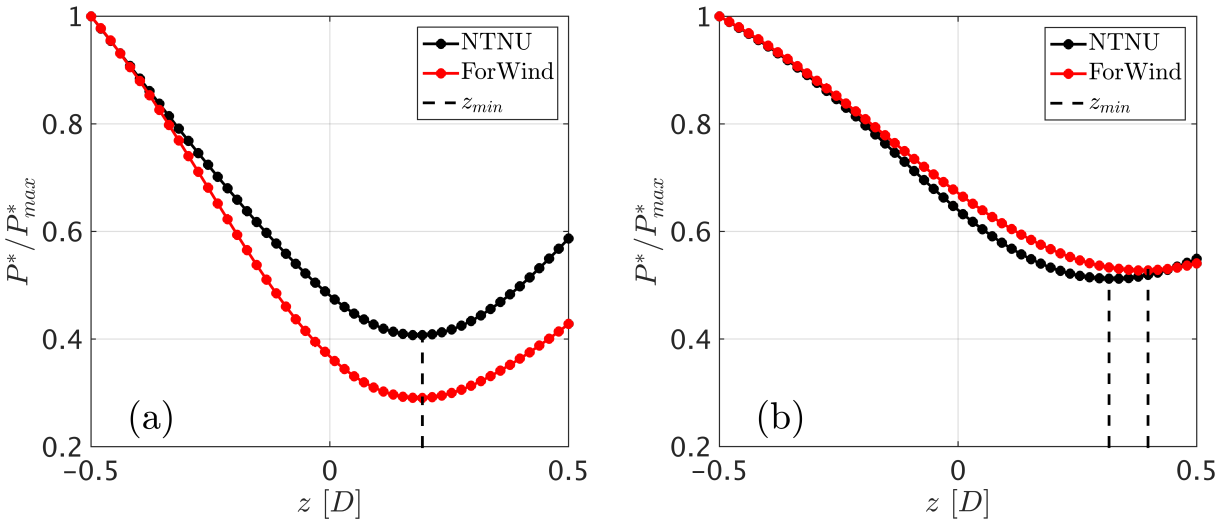

Figure 6. Normalized potential power P^* for various hub locations z of a potential downstream turbine. The respective minimum is marked by the dashed black line. **(a)**: $x/D = 3$, **(b)**: $x/D = 6$. In all cases the yaw angle was $\gamma = -30°$.

nacelle as compared to the NTNU turbine. Further downstream at x/D=6, the deflections are larger, as expected due to the wakes' expansion. However, differences between both turbines become apparent. The wake of the NTNU turbine is located at z/D=0.32, resulting in a slightly smaller skew of approximately 3.0°. The wake behind the ForWind turbine, on the other hand, is deflected slightly further to z/D=0.40, which corresponds to a skew of nearly 3.8° and is therewith nearly constant as compared to the distance x/D = 3.

5. Discussion

The fact that at x/D=3 the same wake deflection in z-direction is observed for both turbines having a different blade design and turbine geometry suggests that those aspects do not influence the wake trajectory at this distance. Further, it is assumed that wind tunnel effects such as blockage or wall-effects are insignificant for both turbines.

At x/D=6, however, differences in the wake deflections of both turbines can be observed, the wake behind the ForWind turbine is found to be deflected slightly further. A possible reason for this is a bigger influence of the increased wind tunnel blockage ratio of the 1.5 times bigger NTNU rotor. While the interaction of the flow behind the ForWind rotor with the wind tunnel side walls (blockage ratio 5.4%) is deemed to be insignificant, the considerably higher blockage ratio of 13% for the the NTNU rotor might influence the wake expansion and defection. Chen et al. [18] quantified the influence of blockage effects in a wind tunnel study, suggesting that those can be neglected for a blockage ratio below 10 %. This finding supports the assumption that blockage effects are of greater relevance for the NTNU turbine and might cause the differences in wake deflection at x/D=6 as the blockage ratios of both turbines are on either side of the suggested 10% limit.

In general, the observed deflections at x/D=3 and x/D=6 are in very good agreement with large eddy simulations (LES) by Vollmer et al. [17] of a full-scale scenario investigating the wake deflection behind a NREL 5MW turbine in stable atmospheric conditions. There, wake deflections of approximately $0.3 - 0.38$ D were observed, depending on the tracking method. Further, an experimental study based on particle image velocimetry (PIV) measurements behind a significantly smaller model wind turbine of 0.15 m rotor diameter showed a very similar wake deflection

at $\gamma = 30\,^\circ$ and x/D=6, being $z/D \approx 0.34$ as reported by Bastankhah and Porté-Agel [3], which is in very good accordance with the current measurements. Another LES study performed by Fleming et al. [19] finds a slightly higher wake deflection of about 0.47 D at a downstream distance of x/D = 6. A recent study by Howland et al. [4] report a wake deflection of $0.40 - 0.55$ D behind a drag disc showing a somewhat bigger deflection. Summarized, the current experiments show that the setup and wake tracking method applied deliver very similar results as for much smaller model wind turbines on the one hand, and simulations of a full-scale turbine on the other hand.
It should be noted that the thrust force of both turbines is a parameter influencing the wake deflections and trajectories, which is, however, not included in this study.

6. Conclusion & future work

A comparative study of the wake deflection behind two different model wind turbines operated in $\gamma = -30^\circ$ yaw misalignment was realized. A very similar defection behavior of the mean wake flow behind the two turbines was observed, resulting in skew angles of $3.0 - 3.8^\circ$. Only insignificant differences in wake deflection were found at x/D=6, although model turbines of different sizes, rotor designs, and geometries were used.
As the deflection magnitudes and skew angles are furthermore observed to fit well with previous experiments on even smaller scale turbines [3] as well as simulations on full-scale turbines [19, 17], general estimations for the deflection can be deducted. Further, it can be concluded that the presented experimental setup and methods allow for a systematic investigation of wake details including their trajectories.
In future analyses of the acquired data, the wake shapes and trajectories will be further analyzed in detail. Besides effects of the turbine geometry, the influence of turbulence and shear in the inflow will be investigated. Moreover, a blind test comparison of the wake data with computational wake simulations of the wind tunnel setup is initiated.

Acknowledgments

The Authors thank Stefan Ivanell for proving the rotor blade design of the ForWind model turbine used in this study as well as the Reiner Lemoine Stiftung (RLS) for funding parts of this work.

References

[1] Medici D and Alfredsson P H 2006 *Wind Energy* **9** 219–236 ISSN 10954244
[2] Krogstad P Å and Adaramola M S 2012 *Wind Energy* **15** 743–756 ISSN 10954244 URL http://doi.wiley.com/10.1002/we.502
[3] Bastankhah M and Porté-Agel F 2016 *Journal of Fluid Mechanics* **806** 506–541 ISSN 0022-1120 URL http://stacks.iop.org/1742-6596/625/i=1/a=012014
[4] Howland M F, Bossuyt J, Martínez-Tossas L A, Meyers J and Meneveau C 2016 *Journal of Renewable and Sustainable Energy* **8** ISSN 19417012 URL http://dx.doi.org/10.1063/1.4955091
[5] Bartl J and Sætran L 2017 *Wind Energy Science* **2** 55–76 URL http://www.wind-energ-sci.net/2/55/2017/
[6] Tong W 2010 *Wind power generation and wind turbine design* (WIT press)
[7] Hsu S, Meindl E A and Gilhousen D B 1994 *Journal of Applied Meteorology* **33** 757–765
[8] Schottler J, Hölling A, Peinke J and Hölling M *Journal of Physics: Conference Series* 072030 ISSN 1742-6588
[9] Odemark Y and Fransson J H M 2013 *Experiments in Fluids* **54** ISSN 07234864
[10] Selig M, Guglielmo J, Broeren A and Giguere P 1995 *SoarTech Publications*
[11] Counsil J N N and Goni Boulama K 2013 *Journal of Aircraft* **50** 204–216 ISSN 0021-8669 URL http://arc.aiaa.org/doi/abs/10.2514/1.C031856
[12] Sætran L and Bartl J 2015 *Technical report NTNU*
[13] Somers D M 2005 THe S825 and S826 Airfoils, Technical Report NREL/SR-500-36344 https://wind.nrel.gov/airfoils/Documents/S825,S826_Design.pdf (last access: 9 February 2017)

[14] Sarmast S and Mikkelsen R F 2012 The experimental results of the NREL S826 airfoil at low Reynolds numbers http://www.diva-portal.org/smash/record.jsf?pid=diva2%3A615785&dswid=-528 (last access: 9 February 2017)
[15] Ostovan Y, Amiri H and Uzol O 2013 *Conference on Wind Energy Science and Technology-RUZGEM*
[16] Sukumar N 1997 *Theoretical and Applied Mechanics, Northwestern University, IL 60208*
[17] Vollmer L, Steinfeld G, Heinemann D and Kühn M 2016 *Wind Energy Science* **1** 129–141 ISSN 2366-7451 URL http://www.wind-energ-sci.net/1/129/2016/
[18] Chen T Y and Liou L R 2011 *Experimental Thermal and Fluid Science* **35** 565–569 ISSN 08941777 URL http://dx.doi.org/10.1016/j.expthermflusci.2010.12.005
[19] Fleming P, Gebraad P M, Lee S, van Wingerden J W, Johnson K, Churchfield M, Michalakes J, Spalart P and Moriarty P 2015 *Wind Energy* **18** 2135–2143 ISSN 10954244 URL http://doi.wiley.com/10.1002/we.1810